

See discussions, stats, and author profiles for this publication at: <https://www.researchgate.net/publication/255713670>

Ultralow Percolation Threshold in Aerogel and Cryogel Templated Composites

ARTICLE *in* LANGMUIR · AUGUST 2013

Impact Factor: 4.46 · DOI: 10.1021/la4017307 · Source: PubMed

CITATIONS

7

READS

62

4 AUTHORS, INCLUDING:



Fahmida Irin

Texas Tech University

24 PUBLICATIONS 303 CITATIONS

SEE PROFILE



Sriya Das

Texas Tech University

18 PUBLICATIONS 349 CITATIONS

SEE PROFILE



Francis Atore

Texas Tech University

2 PUBLICATIONS 29 CITATIONS

SEE PROFILE

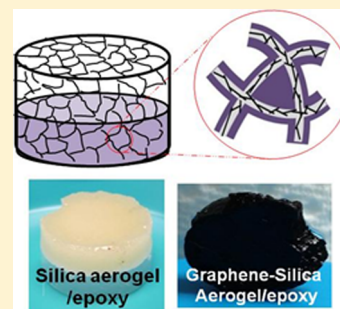
Ultralow Percolation Threshold in Aerogel and Cryogel Templated Composites

Fahmida Irin, Sriya Das, Francis O. Atore, and Micah J. Green*

Department of Chemical Engineering, Texas Tech University, Lubbock, Texas 79409, United States

S Supporting Information

ABSTRACT: We demonstrate a novel concept for preparing percolating composites with ultralow filler content by utilizing nanofiller-loaded aerogel and cryogels as a conductive template. This concept is investigated for several porous systems, including resorcinol-formaldehyde (RF), silica, and polyacrylamide (PAM) gels, and both graphene and carbon nanotubes are utilized as nanofiller. In each case, a stable, aqueous nanofiller dispersion is mixed with a sol-gel precursor and polymerized to form a hydrogel, which can then be converted to an aerogel by critical point drying or cryogel by freeze-drying. Epoxy resin is infused into the pores of the gels by capillary action without disrupting the monolithic structure. We show that conductive graphene/epoxy composites are formed with a very low graphene loading; a percolation threshold as low as 0.012 vol % is obtained for graphene-RF cryogel/epoxy composite. This is the lowest reported threshold of any graphene-based nanocomposites. Similar values are achieved in other aerogel and nanofiller systems, which demonstrates the versatility of this method.



1. INTRODUCTION

One of the chief applications for nanomaterials such as graphene and carbon nanotubes (CNTs) is conductive filler for polymer composites. The goal in these cases is to enhance electrical conductivity even at low nanofiller content. Generally, this is optimized through uniform distribution of the nanomaterial throughout the polymer matrix and by avoiding aggregation. Our group has studied this question in some detail for pristine graphene.^{1–3} A number of processing techniques have aimed to generate homogeneous dispersion of graphene in composites; these typically involve mixing of graphene in polymer solutions, thermoset resins, or even solid polymer powders.^{4–9} Here we examine an alternative concept where the nanomaterial is not homogeneously dispersed; instead a localized network is formed using nanomaterial-loaded aerogels and cryogels as a composite template.

In recent years, three-dimensional (3D) porous graphene structures have generated interest for high surface area applications, particularly in electrodes. A range of techniques have been reported regarding the fabrication of such structures, including template-directed chemical vapor deposition (CVD) of graphene onto nickel foam^{10–12} and graphene-based aerogels.^{13–18} The most common procedure for creating graphene aerogels is to make graphene hydrogels by mild reduction of graphene oxide (GO) and simultaneous self-assembly of reduced graphene oxide (rGO) into a monolithic gel or paste. Subsequent freeze-drying or critical point drying (CPD) of these structures yields aerogels with high porosity and surface area.^{13–16} Alternatively, GO may be dispersed in a polymer hydrogel precursor. After forming the hydrogel and subsequent aerogel, pyrolysis allows for the creation of a graphene-enhanced carbon aerogel with high conductivity.¹⁷

Graphene aerogel formation by directly cross-linking rGO sheets has also been reported.¹⁸ However, prior studies on fabrication of 3D porous graphene structure are invariably based on GO and rGO; one exception is a recent study by Markovic et al. who used the resorcinol-formaldehyde (RF) method to create a carbon aerogel containing polyvinylpyrrolidone (PVP)-stabilized graphene.¹⁹

Here, we report the creation of conductive epoxy nanocomposites by infiltrating Bisphenol-A-based epoxy resins into graphene-loaded aerogel templates. This technique yields ultralow values for the percolation threshold because of the aerogel-based patterning. The central concept is to incorporate graphene into the skeleton of the aerogels to make a conductive network inside an aerogel scaffold before infiltrating the scaffold with epoxy resin, thus creating a graphene network within a porous aerogel network within a bulk composite. We also prepared multiwalled carbon nanotube (MWNT)-loaded aerogel/epoxy composite; which demonstrates that this approach can in principle be extended to various conductive nanomaterial-aerogel-thermoset combinations. rGO-RF/epoxy composites were also prepared for comparison with the pristine graphene composites.

Aerogels have, on occasion, also been used as composite fillers, but this typically involves the creation of an aerogel followed by crushing the aerogel and dispersing it in a composite precursor.^{20–25} This strategy aims to use aerogels simply as a nanofiller source. However, a handful of papers have examined the intriguing concept of backfilling aerogels with

Received: May 6, 2013

Revised: August 6, 2013

Published: August 8, 2013



polymer and other molecules so that the aerogel may serve directly as a filler skeleton in the composite.^{10,26–28} Examples include recent work from Kim et al., who backfilled CNT aerogels with poly(dimethyl siloxane) (PDMS) to create stretchable conductors.²⁶ In another study, Chen et al. infiltrated PDMS into a CVD-grown graphene foam for electronic applications.¹⁰ Gui et al. infused epoxy resin into a CVD-grown CNT forest to form a conductive CNT/epoxy composite system.²⁷ Several studies have attempted to reinforce the aerogel with polymer in both hydrogel and aerogel stage; the purpose was only to increase the strength of the resulting aerogel.^{29,30} To our knowledge, ours is the first study that focuses on backfilling a thermoset into a pre-existing composite aerogel scaffold in order to prepare an ultralow percolation threshold composite.

2. EXPERIMENTAL SECTION

Materials. Expanded graphite (EG) was provided by Asbury Carbon (CAS # 7782-42-5, grade 3805). Multiwalled carbon nanotubes (MWNTs) were purchased from Cheap Tubes, Inc. (Brattleboro, VT). The outer diameter of these tubes were 30–50 nm and length ~10–20 μm with >95 wt % purity and 1.5 wt % ash content. Graphene and nanotube stabilizers, i.e., polyvinylpyrrolidone (PVP) (M_w : 10^3 g/mol), 1-pyrenesulfonic acid sodium salt (PSA), and polyacrylamide (PAM) (M_w : 10^5 g/mol) were purchased from Sigma Aldrich.

Acrylamide (AM) (purity $\geq 99.99\%$), *N*-methylbisacrylamide (MBA), and potassium persulfate (KPS) (purity $\geq 99.99\%$) were purchased from Sigma Aldrich, which acts as a cross-linker and initiator respectively for making PAM cryogel.

1,3-Benzenediol (resorcinol, purity $\geq 99\%$), formaldehyde (36.5–38% in H_2O), and sodium carbonate (purity $\geq 99\%$) were purchased from Sigma Aldrich for the preparation of RF cryogel.

Silica gel forming reagents, i.e., tetraethyl orthosilicate (TEOS) (99.999% trace metals basis, density: 0.933 g mL^{-1}), ammonium hydroxide (28–30 wt % in water), and ammonium fluoride ($\geq 99.99\%$ trace metals basis) were also bought from Sigma Aldrich.

A bisphenol A-based epoxy (Epoxy 2000) resin and 2120 epoxy hardener were purchased from Fibreglast, USA for the preparation of the composite. Epoxy 2000 (Part-A) is multifunctional acrylate and 2120 epoxy hardener (Part-B) is mixture of amines. A high performance epoxy can be prepared by mixing Part-A and Part-B at a certain ratio and curing it for 2 h. Water-soluble epoxy resin (Bisphenol A diglycidyl ether) and the curing agent (pentacrythritol tetrakis (3-mercaptopropionate)) were purchased from sigma Aldrich. All of these chemicals were used without any further treatment.

Preparation of Graphene and MWNT Dispersion. Separate pristine graphene aqueous dispersions were prepared using two different stabilizers (PSA and PVP) by noncovalent functionalization. A specific amount of stabilizer was dissolved into 50 mL of deionized water (DI); the concentration of PSA and PVP in the solution was 3 mg mL^{-1} and 10 mg mL^{-1} respectively. 50 mg mL^{-1} expanded graphite (EG) was added to this solution and tip sonicated for 1.5 h. The dispersion was then centrifuged (Centrifuge 225, Fischer Scientific) at 5000 rpm for 4 h to remove larger aggregates. The supernatant was collected after centrifugation, and UV–vis absorbance was performed on the graphene dispersion in Shimadzu UV–vis spectrophotometer-2550 at a wavelength of 660 nm; the concentration of graphene was calculated by Lambert–Beer’s law. The extinction coefficient for graphene in PSA and PVP aqueous solution was determined previously as 1490 $\text{mL mg}^{-1} \text{m}^{-1}$ and 1293 $\text{mL mg}^{-1} \text{m}^{-1}$ respectively.^{3,31} The details of calculating extinction coefficient and the stability study of the graphene dispersions using PVP and PSA stabilizers are described in our prior papers. The TEM images in our prior studies suggest that the graphene prepared after sonication and centrifugation are single to few layer thick.^{3,31} The TEM images on graphene/PVP and graphene/PSA dispersions are given in the Supporting Information. Similarly, a PAM stabilized MWNT

dispersion was also prepared; the extinction coefficient of PAM solution was determined as 575 $\text{mL mg}^{-1} \text{m}^{-1}$.

Synthesis of Graphene/RF Cryogel. Resorcinol (17.2 mg mL^{-1}), formaldehyde (25 mg mL^{-1}), and sodium carbonate catalyst (0.082 mg mL^{-1}) were added to a certain volume of aqueous graphene/PSA dispersion (0.6 mg mL^{-1}) and dissolved completely (resorcinol-to-catalyst molar ratio (R/C) was 200). The sol–gel mixture was then kept into a sealed glass vial and polymerized in an oven at 90 $^\circ\text{C}$ for 2 days. After completing the polycondensation reaction, the graphene/RF hydrogel was formed, which was flash frozen into liquid nitrogen and freeze-dried to make the cryogel. The graphene content of the as prepared cryogel was 1.4 wt %. A control sample with no graphene was also prepared with the same composition of reagents for comparison.

Synthesis of Graphene/Silica Aerogel. Silica and graphene-silica aerogel were prepared by the base-catalyzed TEOS method. Preparation of graphene-silica aerogel consists of making three separate solutions and mixing them in proper ratio. The “stock solution” was prepared by mixing 0.926 g of ammonium fluoride and 10.25 g of ammonium hydroxide in 50 mL of water. TEOS (2.35 g) was dissolved in 5 mL of ethanol to make the “alkoxide solution”. Water (3.5 mL) and 5 mL of ethanol were mixed in a beaker, and 5–6 drops of stock solution was added to it; this is the “catalyst solution”. This catalyst solution was mixed with the alkoxide solution, which is called the “sol-gel mixture”. The mixture was then poured into a sealed vial for gelation; the gel formed within 10 min after mixing. PVP stabilized graphene dispersion was used to make the graphene-silica gel instead of graphene/PSA dispersion.

Synthesis of MWNT/PAM Cryogel. AM (33 mg mL^{-1}), MBA (5.22 mg mL^{-1}), and KPS (25 mg mL^{-1}) were dissolved in the stabilized MWNT/PAM dispersion. This solution was left in the oven at ~ 70 $^\circ\text{C}$; the hydrogel started forming after 2 h. The gel was aged for 24 h for complete polymerization and then freeze-dried after flash freezing into liquid nitrogen to obtain MWNT-PAM cryogel. Comparison against the baseline was done by preparing PAM cryogel with no graphene.

Preparation of Epoxy Composite. Epoxy curing agent (2120 epoxy hardener) was added to the resin at 0.27:1 weight ratio and mixed properly. The aerogels were dipped into the epoxy bath for infiltration. Epoxy resin has a pot life of 120 min after mixing with hardener; however, the time of infusion into the aerogel is fast enough to avoid premature curing. After complete infusion, the aerogel was cured in a vacuum oven at 60 $^\circ\text{C}$ for making the ultralow percolation composite. Graphene and MWNT content in the final composite was calculated by dividing the mass of nanofiller by the total mass of aerogel and cryogel matrix (RF, silica or PAM), epoxy, and the filler.

Characterization. The morphology of the aerogels was characterized by scanning electron microscopy (SEM) and transmission electron microscopy (TEM) images. SEM was performed on a HITACHI S4300 electron microscope after sputter coating with Au/Pd in a Hummer V technics sputter coater. The images were taken using an acceleration voltage of 5 KV and at working distance of 8–15 mm. TEM was conducted on silica and graphene-silica aerogel on a HITACHI H8100 electron microscope at an accelerating voltage of 75 KV; the crushed powdered sample was spread onto a HC200-CU grid for TEM imaging. Electrical conductivity was determined by a standard four-point probe method; there was one current source meter (Keithley 2400) and one voltmeter (Keithley 2000) connected to the four-point probe (Signatone, SP4–40045TBY) to measure the resistivity of the material. In-plane electrical resistivity was measured at least three times on each sample, and the average data was taken to calculate the conductivity. Physiosorption analysis was performed on an Autosorb iQ machine (Quantachrome Instruments) to determine the surface area of the aerogels. All the aerogel samples were degassed for 15 h at 90–100 $^\circ\text{C}$ before acquiring the nitrogen adsorption–desorption isotherm. Multipoint Brunauer–Emmett–Teller (BET) method was applied to the isotherm to determine the surface area of the samples.

Scheme 1. Composite Fabrication of Aerogel Scaffolds

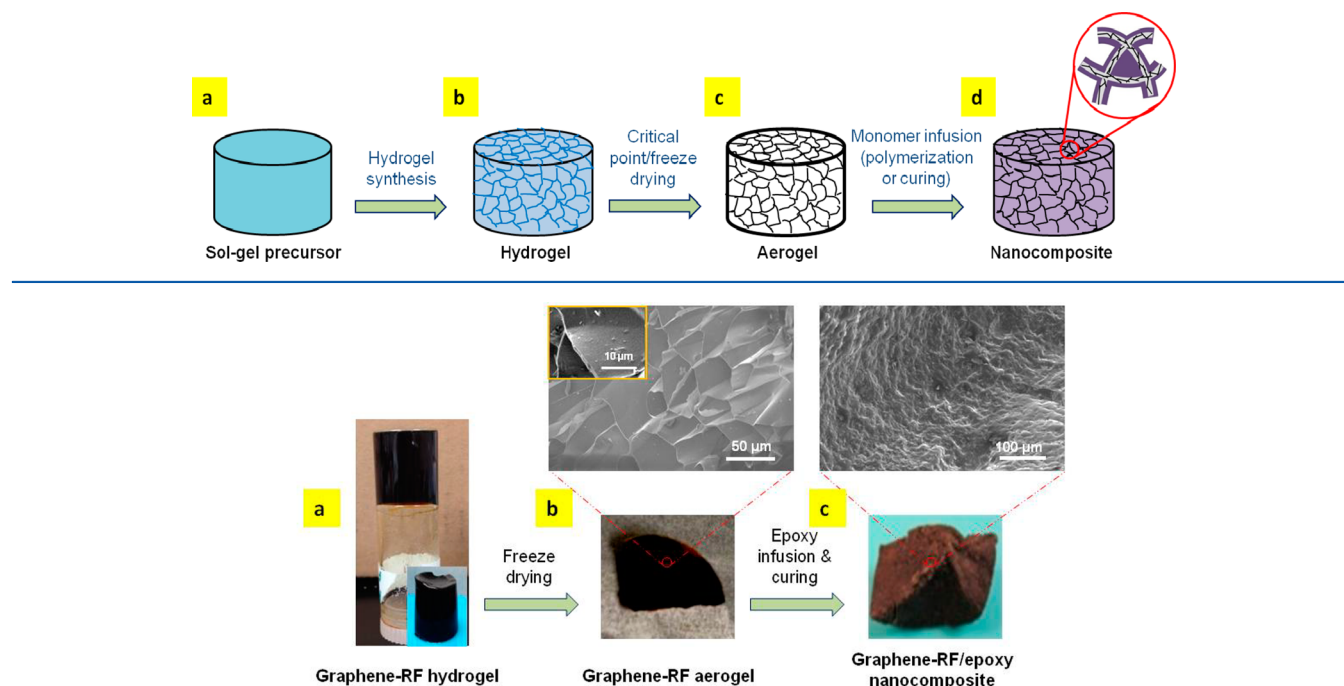


Figure 1. Production of graphene-RF cryogel and graphene-RF/epoxy composite. (a) Graphene-RF hydrogel prepared by polycondensation reaction. (b) SEM image on 1.4 wt % graphene-RF cryogel showing the porous structure. The inset in the SEM image is a magnified view of the skeleton. (c) SEM on 0.03 wt % (0.012 vol %) graphene-RF/epoxy composite confirms the infusion and curing of epoxy inside the pores of the cryogel.

3. RESULTS AND DISCUSSION

The procedure for making conductive composites using nanomaterial-loaded aerogels as a scaffold is depicted in Scheme 1. In a typical aerogel synthesis, a sol–gel precursor (Scheme 1a) is allowed to form a monolithic gel (Scheme 1b); the gel forms a three-dimensional cross-linked network within the solvent (water or organic solvent) by physical or chemical bonds. We incorporate a nanomaterial into this gel by introducing a stable nanomaterial dispersion prior to cross-linking. The gel is then subjected to drying (either by freeze-drying or CPD) to remove the liquid from the pores. Therefore, the resulting aerogel structure (Scheme 1c) has high porosity and large surface area. The last step is to construct the nanocomposite by infiltration and subsequent curing of monomer material or epoxy resin in the pores of the gel. This step does not disrupt the connectivity (and conductivity) of the nanofiller network inside the aerogel.

The magnified schematic of the pore structure of the aerogel (Scheme 1d) illustrates the mechanism of nanofiller percolation within the aerogel skeleton. Three cocontinuous hierarchical structures are formed in the process of making the composites: one is the interconnected fillers inside the pore walls of the aerogels, the second one is the skeleton network, and the last one is the infiltrated polymer matrix. Consequently, an electrically insulating organic, inorganic, or polymer aerogel can turn into an electrically conductive scaffold when those nanofillers are connected throughout the skeleton. Moreover, the low density and large surface area of the aerogel allows for greater adhesion area between the aerogel and the bulk matrix.

This strategy of composite preparation is applied to three different aerogel systems: the first is resorcinol-formaldehyde (RF) (an organic cryogel system), the second is an inorganic

silica aerogel, and the last is a polymeric gel (polyacrylamide (PAM) cryogel). RF and PAM were prepared by freeze-drying and are hence termed as cryogel throughout the paper. On the other hand, silica is referred as aerogel since it was made by CPD. The continuous nanofiller network is the key to achieving percolation at low concentrations in these structures. Previous studies established that such segregated structures are beneficial for creating conductive nanocomposites at a low filler loading.^{7–9,32} Qi et al. achieved a threshold value of 0.075 vol % because of selective localization of graphene in a graphene/polystyrene/polylactic acid ternary composite.⁷ Pang et al. employed hot compression to create a segregated structure of graphene to attain percolation at 0.06 vol % graphene loading in polyethylene composite.⁸ Similar results were reported by Hu et al.⁹ However, by utilizing the graphene aerogel scaffold, we achieved the same conductivity level ($\sim 10^{-7}$ S m⁻¹) in the composite at a graphene loading, which is an order of magnitude lower than the literature value for graphene/epoxy nanocomposite^{33–36} and at least factor of 3 less than other matrices such as polyethylene or polystyrene.⁹

The process of creating epoxy nanocomposites on a graphene-RF cryogel scaffold is demonstrated in Figure 1. A stable 1-pyrenesulfonic acid sodium salt (PSA) stabilized graphene dispersion (0.6 mg mL⁻¹) was mixed with the RF solution. The catalyst (sodium carbonate) was added to the reaction mixture and placed in an electric oven at 90 °C for hydrogel formation. The graphene-RF hydrogel (Figure 1a) was then flash frozen in liquid nitrogen and freeze-dried to form an RF cryogel with 1.4 wt % graphene. The morphology of the pore structure of graphene-RF and RF cryogels is shown in the SEM images in Figure 1b and Figure S1 (Supporting Information), respectively. The graphene-RF cryogel exhibits a sheet like morphology with large pores (pore size 20–50

μm), whereas the RF cryogel has comparatively smaller pores (pore size $\sim 15\text{--}20\ \mu\text{m}$). Moreover, the skeleton of the graphene-RF cryogel is rough compared to the smooth surface of the RF cryogel (Figure S1c). This irregular surface morphology is due to the presence of graphene sheets in the pore walls. The inset of the SEM images in Figure 1b shows the magnified portion of the skeleton where graphene is protruding out from the surface. The evidence of the formation of graphene network is given in the supporting document (Figure S2). The nitrogen adsorption–desorption isotherm of the RF cryogel (Figure S3a) shows a type II isotherm, which is the characteristic curve for macroporous materials (pore size $>50\ \text{nm}$). Moreover, a type H4 hysteresis was observed, which indicates the presence of micropores as well. The application of density functional theory (DFT) to this data suggests the presence of micropores in $0.7\text{--}1.5\ \text{nm}$ range. Some mesopores are also present in the range of $2\text{--}18\ \text{nm}$. This hierarchical pore structure of RF cryogel is in agreement with prior literature.^{37,38} The RF cryogel has high surface area ($\sim 615\ \text{m}^2\ \text{g}^{-1}$) and low density ($\sim 17\ \text{mg}\ \text{cm}^{-3}$), but the surface area decreases with the addition of $1.4\ \text{wt}\%$ graphene ($\sim 374\ \text{m}^2\ \text{g}^{-1}$) while the density increases ($\sim 25\ \text{mg}\ \text{cm}^{-3}$). These values of surface area are comparable to the prior literature.^{17,18,39} The electrical conductivity of the $1.4\ \text{wt}\%$ graphene-RF cryogel is $2 \times 10^{-6}\ \text{S}\ \text{m}^{-1}$, which provides the confirmation that graphene sheets are interconnected throughout the RF cryogel scaffold.

The conductive graphene-RF/epoxy composite was prepared by soaking the graphene-RF cryogel in an epoxy bath for infiltration and by curing it in an electric oven at $65\ ^\circ\text{C}$ for 6 h. Pictures of the cryogel during epoxy infusion are presented in Figure S4b. The graphene content in the final composite is $0.03\ \text{wt}\%$ ($0.012\ \text{vol}\%$). The conductivity of the composite is $2.56 \times 10^{-7}\ \text{S}\ \text{m}^{-1}$; thus, the percolation threshold itself will be lower than this value. This is the lowest reported percolation threshold of any graphene-based composites by any technique as mentioned above. The conductivity of the composite demonstrates that the graphene network remain intact even after infusion of epoxy into the scaffold. Figure 1c shows the SEM image on the fracture surface of the $0.012\ \text{vol}\%$ graphene-RF/epoxy composite. The images were taken in different areas of the fracture surface of the composite, and no open pores were observed, which suggests complete infiltration and curing of epoxy inside the pores of the aerogel template. In addition to the SEM images, nitrogen adsorption–desorption analysis was also performed. A large decrease in surface area ($23\ \text{m}^2\ \text{g}^{-1}$) suggests the effectiveness of backfilling into the cryogel (see supporting Figure S5).

To study the effect of increasing graphene content on electrical conductivity, a higher graphene loaded ($5\ \text{wt}\%$) RF cryogel was prepared. After epoxy infusion, the graphene content becomes $0.2\ \text{wt}\%$ ($0.078\ \text{vol}\%$); the conductivity of this composite reaches $4.6 \times 10^{-5}\ \text{S}\ \text{m}^{-1}$, significantly higher than the insulating epoxy matrix and 2 orders of magnitude higher than the conductivity at percolation threshold ($0.012\ \text{vol}\%$). This would be expected in a bulk, percolating composite sample prepared by homogeneous mixing of filler in the matrix; but here we show a similar trend inside the aerogel skeleton. For comparison with pristine graphene, an rGO-RF/epoxy composite (Figure S6) was also prepared; the percolation threshold in this system is obtained at $0.06\ \text{wt}\%$ ($0.023\ \text{vol}\%$), and the conductivity value is $3.73 \times 10^{-8}\ \text{S}\ \text{m}^{-1}$ (details are given in the Supporting Information, Section S6).

The second system of interest was graphene-silica aerogels (Figure 2). The hydrogels (Figure S7) were prepared by the

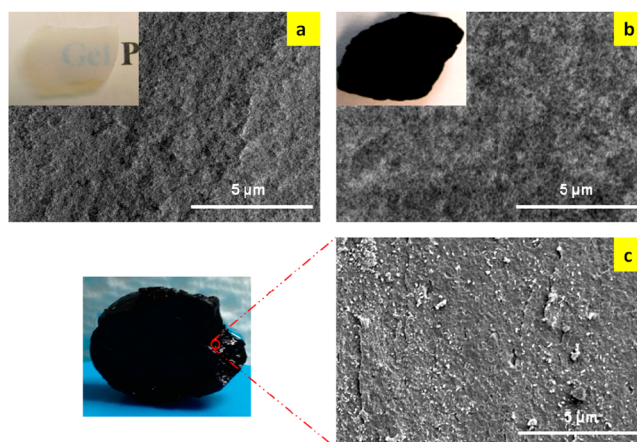


Figure 2. SEM images showing the morphology of (a) silica, (b) $0.3\ \text{wt}\%$ graphene-silica, and (c) $0.04\ \text{wt}\%$ ($0.017\ \text{vol}\%$) graphene-silica/epoxy composite. The SEM images on silica and graphene-silica aerogels suggest that the surface morphology of the aerogel is unaffected by graphene loading. SEM on the fracture surface of the epoxy composite (c) demonstrates that the pores are filled with epoxy.

base-catalyzed TEOS method, and the aerogels were formed by CPD. PVP-stabilized graphene dispersions were used in synthesizing the initial graphene-silica hydrogel. Figure 2a and 2b show the SEM images of silica and graphene-silica aerogels, respectively. SEM images show that both silica and graphene-silica aerogels have similar morphologies. Silica aerogels tend to form nanometer size pores and TEM images (Figure S8) on silica and graphene-silica aerogels prove that incorporation of graphene into the silica aerogel did not alter its mesoporous structure. The nitrogen adsorption–desorption isotherm (Figure S3c and S3d) of the aerogels show type III behavior (convex to the relative pressure, P/P_0) with a hysteresis loop of H3 type (according to IUPAC classification of hysteresis loop). At high P/P_0 , the hysteresis loop does not exhibit any limiting adsorption, which is typically associated with H3 hysteresis. From the DFT analysis, the pore size of the silica and graphene-silica aerogels were found in the range of $2\text{--}10\ \text{nm}$, which is in agreement with the mesoporous structure observed in the TEM image. Silica aerogel has the highest BET surface area ($\sim 1410\ \text{m}^2\ \text{g}^{-1}$) of the systems studied in this paper. Addition of graphene into silica aerogel lowers the surface area ($\sim 1150\ \text{m}^2\ \text{g}^{-1}$) and increases the density ($\sim 124\ \text{mg}\ \text{cm}^{-3}$). However, this value is much higher than that of graphene-RF aerogel prepared by freeze-drying. It is already established from prior literature that aerogel prepared by CPD has larger surface area compared to freeze-drying. The large surface area allows for an extended, connected graphene network inside the silica; electrical conductivity measurements ($2.9 \times 10^{-6}\ \text{S}\ \text{m}^{-1}$) at $0.3\ \text{wt}\%$ graphene loading confirm this to be the case.

The graphene-silica/epoxy composite was prepared similarly as mentioned above. The backfilling of the resin happened within a minute by capillary forces because of the mesoporous structure of graphene-silica aerogel. Figure S4c shows the digital camera image of a silica aerogel (no graphene) with partially infused epoxy into it. Because of the transparent nature of silica aerogel, the backfilling of epoxy into the pores is visible, which illustrates the ease of infiltration; graphene-silica aerogel

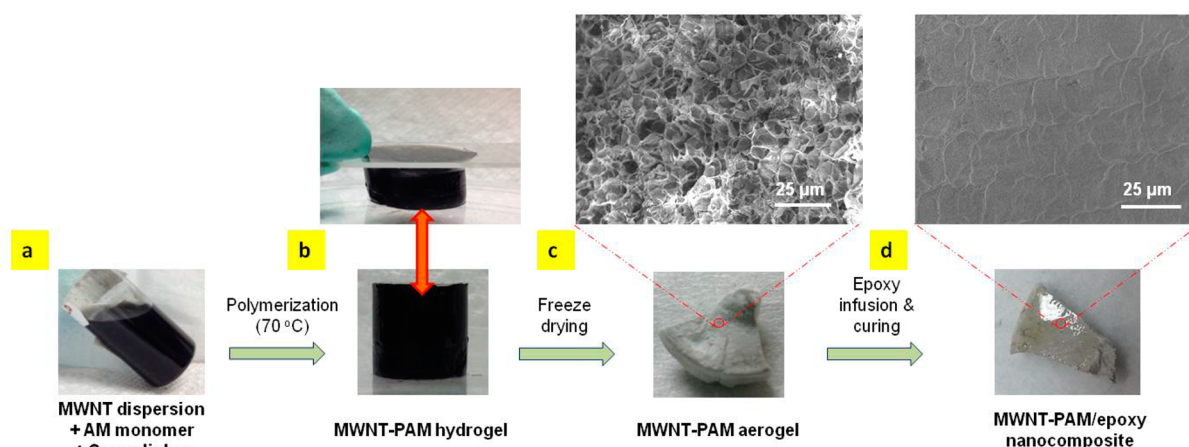








Figure 3. The epoxy nanocomposite production is shown for a MWNT-PAM cryogel template. Digital camera images of (a) PAM hydrogel precursors mixed with a MWNT-PAM dispersion, (b) elastic MWNT-PAM hydrogel prepared by in situ polymerization at 70 °C, and (c) MWNT-PAM cryogel created by flash freezing in liquid nitrogen and freeze-drying. The SEM image shows the porous structure of the cryogel and (d) the epoxy-infused MWNT-PAM cryogel; the SEM image on the fracture surface of the composite shows epoxy filled pores.

Table 1. Summary of the Properties of Different Aerogels and Cryogels with and without Nanofiller and the Electrical Conductivity of the Graphene Aerogels before and after Epoxy Infusion

Type of aerogels	Drying process	Density, mg cm ⁻³	Conductivity, S m ⁻¹	wt. % graphene after epoxy infusion	Conductivity after epoxy infusion, S m ⁻¹	Surface area, m ² g ⁻¹	Pore size*
 RF	Freeze drying	~17	Not conductive	----	----	615	0.7-1.5 nm (DFT) 2-17 nm (DFT) 15-20 μm (SEM)
 1.4 wt. % graphene-RF	Freeze drying	~25	2×10^{-6}	0.03	2.65×10^{-7}	374	0.8-1.6 nm (DFT) 2-18 nm (DFT) 20-50 μm (SEM)
 Silica	CPD	~119	Not conductive	----	----	1410	2-8 nm (DFT)
 0.3 wt. % graphene-silica	CPD	~124	2.9×10^{-6}	0.04	7.16×10^{-7}	1150	2-10 nm (DFT)
 PAM	Freeze drying	~95	Not conductive	----	----	170	0.7-1.3 nm (DFT) 2-13 nm (DFT) 5-10 μm (SEM)
 0.5 wt. % MWNT-PAM	Freeze drying	~138	7.12×10^{-8}	0.086	3.9×10^{-8}	80	0.7-1.4 nm (DFT) 2-15 nm (DFT) 5-10 μm (SEM)

*RF and PAM cryogel systems have hierarchical structures of micropores (<2 nm), mesopores (2–50 nm) and macropores (>50 nm). The micro and mesopores are determined by DFT analysis, and the macropores are found from SEM images.

also displayed similar behavior. SEM image (Figure 2c) on the fracture surface of the composite also demonstrates the effectiveness of epoxy infusion into the aerogel scaffold. Graphene content in the composite after epoxy infusion is 0.04 wt % (0.017 vol %) and the conductivity of the composite

is $7.16 \times 10^{-7} \text{ S m}^{-1}$. The conductivity increases with increasing graphene loading, showing $1.29 \times 10^{-5} \text{ S m}^{-1}$ at 0.3 wt % (0.13 vol %) graphene.

Finally, a polymeric cryogel system (PAM cryogel) was investigated to apply the idea of making conductive nano-

composites by using a porous template (Figure 3). A PAM-stabilized MWNT dispersion (Figure 3a) was used in this case. (Note that a graphene-PAM cryogel system was also studied, with mixed results because of difficulties with PAM as a graphene stabilizer on a per-mass basis. Details are described in the Supporting Information). The MWNT-PAM hydrogel was formed by in situ polymerization of AM (see Experimental Section). The as-prepared gel is flexible and elastic as shown in Figure 3b, similar to conventional PAM hydrogel.⁴⁰ The hydrogel was flash frozen in liquid nitrogen and freeze-dried to yield the MWNT-PAM cryogel (Figure 3c). The surface area of the MWNT-PAM cryogel is lower ($80 \text{ m}^2 \text{ g}^{-1}$) than conventional aerogels, which is a common characteristic of such polymeric aerogels. It is possible that some part of the porous network is disrupting during freeze-drying, which would substantially decrease the surface area.⁴¹ The SEM image of the MWNT-PAM cryogel shows macroporous morphology with pore size ranging from 5 to $10 \mu\text{m}$ (Figure 3c). MWNT-free PAM cryogel has a similar morphology (Figure S9c). The DFT analysis on the isotherm confirms the presence of micropores and mesopores as well; the size of the micropores of this cryogel range from 0.7 to 1.4 nm and the mesopores range from 2 to 15 nm. The creation of a conductive MWNT-PAM cryogel structure is entirely novel. A handful of studies have examined PAM and rGO-PAM hydrogel rheology;^{7,42,43} but none of these studies explored the idea of making an cryogel out of these hydrogels.

A 0.5 wt % MWNT-loaded PAM cryogel was synthesized, and this 3D structure becomes conductive ($7.12 \times 10^{-8} \text{ S m}^{-1}$) at this filler loading. While preparing the composite by backfilling of epoxy, PAM was found to be incompatible with acrylate based epoxy (Epoxy 2000 Bisphenol A) because of the high viscosity and surface tension. Instead, a low-viscosity water-soluble epoxy (Bisphenol A diglycidyl ether) was used. Even after infusion of epoxy, the composite is conductive ($3.9 \times 10^{-8} \text{ S m}^{-1}$), indicating that the interconnected network of MWNT into the pore walls remained intact. The SEM image (Figure 3d) on the fracture surface of the composite also demonstrates that most of the pores are completely filled with epoxy without disrupting the pore walls. Finally, the amount of MWNT in the epoxy composite is 0.086 wt % (0.035 vol %). This result implies that the strategy of creating low percolation composite can be fulfilled even by using a polymeric cryogel system. A conductive graphene-PAM/epoxy composite was fabricated in a similar way, which is described in Figure S10.

A summary of the physical properties of all the aerogel and cryogels with and without nanofiller loading and the conductivity values of the percolating network are presented in Table 1. In the case of graphene-RF cryogel/epoxy composite, a conductive sample is obtained at graphene content as low as 0.03 wt % (0.012 vol %). Silica aerogel also shows great promise in regard to the ultralow percolation threshold composite preparation; after infiltration of epoxy, the sample displays conductivity at values as low as 0.04 wt % (0.017 vol %) graphene loading. Thus, the actual percolation threshold will be slightly lower than these values if fitted by the power law model. These values are the lowest reported percolation threshold for any graphene based composites. The MWNT-PAM aerogel/epoxy composite yields a percolation threshold point as low as 0.086 wt % (0.035 vol %). The table also shows that the density of the aerogels increases and the surface area decreases with nanofiller loading compared to the baseline aerogels. Surface area and pore structure play an

important role in creating a low percolation composite. The high surface area of the aerogels allows for the creation of a composite by taking the advantage of the ultrahigh surface area of the nanofiller. As a result, the surface area of the composites may be maximized in contrast with conventional bulk nanocomposites whose area is orders of magnitude less than the nanofiller.

The ease of epoxy infiltration depends on two main factors: (a) pore size of the aerogel and (b) viscosity and wetting property of the monomer with the aerogel surface. In the case of mesoporous (pore size 2–50 nm) materials such as silica aerogel, epoxy infusion happens rapidly via capillary forces.⁴¹ On the other hand, in macroporous gels (pore size >50 nm), i.e., PAM or RF cryogel (prepared by freeze-drying), capillary forces are relatively weak.⁴¹ (Note that the shape of the samples in all the experiments shows variation for two reasons. Silica aerogels tend to be brittle and delicate. Also, in the case of RF and PAM cryogels, the monolithic structure tends to break during flash freezing into liquid nitrogen.)

One critical point to consider when an aerogel composite is made from a nanofiller dispersion is the stability of the dispersion and the compatibility of the dispersion with the aerogel precursor. Dispersion quality is crucial to achieve a homogeneous distribution of graphene and CNT with the sol-gel mixture as well as to acquire an electrical conductivity from the conductive filler network. Otherwise, the filler might aggregate during the gelation process, which will in turn increase the percolation point.

4. CONCLUSION

In summary, we have demonstrated a new technique to fabricate composites with ultralow percolation threshold using aerogel and cryogel template procedure where an interconnected network of conductive filler can be formed within the porous aerogel. This study also demonstrates that the backfilling of a thermosetting resin or other polymers and elastomers has little effect on the existing segregated structure. The key factor that determines the low percolation threshold in the composite is the original nanomaterial dispersion quality, which ensures the formation of a conductive network extending throughout the skeleton of the aerogel. Moreover, the use of various nanofillers (pristine graphene and MWNT) in three different aerogel and cryogel systems (organic, inorganic, and polymeric) established the versatility of this procedure. We believe that our approach of utilizing the 3D structure of nanofiller loaded aerogel templates will provide a platform for the preparation of lightweight, flexible, and conductive nanocomposites for multifunctional applications.

■ ASSOCIATED CONTENT

Supporting Information

Supporting Information includes pictures of hydrogels, the physisorption analysis, mechanism of epoxy infusion, SEM images on the RF cryogels, TEM images of silica aerogel, TEM on graphene dispersions, and details of graphene-PAM aerogel/epoxy composite. This information is available free of charge via the Internet at <http://pubs.acs.org/>.

■ AUTHOR INFORMATION

Corresponding Author

*E-mail: micah.green@ttu.edu.

Notes

The authors declare no competing financial interest.

ACKNOWLEDGMENTS

We acknowledge Dorsa Parviz, Robert Fullerton, and Shane Metzler for graphene dispersion processing. We are thankful to H. S. Tanvir Ahmed and Dr. Alan F. Jankowski for helping us in aerogel characterization. We acknowledge Sanjoy K. Bhattacharia for helping in thermal treatment of the cryogels. We also appreciate the help from Marauo Davis in CPD operation. The SEM and TEM were performed at the TTU Imaging Center (funded by NSF MRI 04-511) supported by Dr. Mark J. Grimson, Mary Catherine Hastert, and Professor Lauren S. Gollahon. Surface area measurements were conducted in the Materials Characterization Center with the support of Dr. Juliusz Warzywoda and Dr. Al Sacco of TTU. Funding was provided by the U.S. National Science Foundation (NSF) under CAREER award CMMI-1253085 and by the Air Force Office of Scientific Research Young Investigator Program (AFOSR FA9550-11-1-0027).

REFERENCES

- (1) Das, S.; Irin, F.; Tanvir Ahmed, H. S.; Cortinas, A. B.; Wajid, A. S.; Parviz, D.; Jankowski, A. F.; Kato, M.; Green, M. J. Non-covalent functionalization of pristine few-layer graphene using triphenylene derivatives for conductive poly(vinyl alcohol) composites. *Polymer* **2012**, *53*, 2485–2494.
- (2) Wajid, A. S.; Ahmed, H. S. T.; Das, S.; Irin, F.; Jankowski, A. F.; Green, M. J. High-performance pristine graphene/epoxy composites with enhanced mechanical and electrical properties. *Macromol. Mater. Eng.* **2013**, *298*, 339–347.
- (3) Wajid, A. S.; Das, S.; Irin, F.; Ahmed, H. S. T.; Shelburne, J. L.; Parviz, D.; Fullerton, R. J.; Jankowski, A. F.; Hedden, R. C.; Green, M. J. Polymer-stabilized graphene dispersions at high concentrations in organic solvents for composite production. *Carbon* **2012**, *50*, 526–534.
- (4) Rafiee, M. A.; Rafiee, J.; Wang, Z.; Song, H.; Yu, Z.-Z.; Koratkar, N. Enhanced mechanical properties of nanocomposites at low graphene content. *ACS Nano* **2009**, *3*, 3884–3890.
- (5) Yin, S.; Rong, C.; Zhang, S.; Huo, P.; Wang, G. The preparation and electrical properties of the functionalized graphene/poly(ether sulfone) nanocomposites. *High Perform. Polym.* **2011**, *23*, 592–601.
- (6) Chen, D.; Wang, X. Y.; Liu, T. X.; Wang, X. D.; Li, J. Electrically conductive poly(vinyl alcohol) hybrid films containing graphene and layered double hydroxide fabricated via layer-by-layer self-assembly. *ACS Appl. Mater. Interfaces* **2010**, *2*, 2005–2011.
- (7) Qi, X.-Y.; Yan, D.; Jiang, Z.; Cao, Y.-K.; Yu, Z.-Z.; Yavari, F.; Koratkar, N. Enhanced electrical conductivity in polystyrene nanocomposites at ultra-low graphene content. *ACS Appl. Mater. Interfaces* **2011**, *3*, 3130–3133.
- (8) Pang, H.; Chen, T.; Zhang, G.; Zeng, B.; Li, Z.-M. An electrically conducting polymer/graphene composite with a very low percolation threshold. *Mater. Lett.* **2010**, *64*, 2226–2229.
- (9) Hu, H.; Zhang, G.; Xiao, L.; Wang, H.; Zhang, Q.; Zhao, Z. Preparation and electrical conductivity of graphene/ultrahigh molecular weight polyethylene composites with a segregated structure. *Carbon* **2012**, *50*, 4596–4599.
- (10) Chen, Z. P.; Ren, W. C.; Gao, L. B.; Liu, B. L.; Pei, S. F.; Cheng, H. M. Three-dimensional flexible and conductive interconnected graphene networks grown by chemical vapour deposition. *Nat. Mater.* **2011**, *10*, 424–428.
- (11) Huang, X.; Qian, K.; Yang, J.; Zhang, J.; Li, L.; Yu, C.; Zhao, D. Functional Nanoporous Graphene Foams with Controlled Pore Sizes. *Adv. Mater.* **2012**, *24*.
- (12) Cao, X.; Shi, Y.; Shi, W.; Lu, G.; Huang, X.; Yan, Q.; Zhang, Q.; Zhang, H. Preparation of Novel 3D Graphene Networks for Supercapacitor Applications. *Small* **2011**, *7*, 3163–3168.
- (13) Chen, W.; Li, S.; Chen, C.; Yan, L. Self-assembly and embedding of nanoparticles by in situ reduced graphene for preparation of a 3D graphene/nanoparticle aerogel. *Adv. Mater.* **2011**, *23*, S679.
- (14) Chen, W.; Yan, L. In situ self-assembly of mild chemical reduction graphene for three-dimensional architectures. *Nanoscale* **2011**, *3*, 3132–3137.
- (15) Zhang, X. T.; Sui, Z. Y.; Xu, B.; Yue, S. F.; Luo, Y. J.; Zhan, W. C.; Liu, B. Mechanically strong and highly conductive graphene aerogel and its use as electrodes for electrochemical power sources. *J. Mater. Chem.* **2011**, *21*, 6494–6497.
- (16) Cong, H.-P.; Ren, X.-C.; Wang, P.; Yu, S.-H. Macroscopic multifunctional graphene-based hydrogels and aerogels by a metal ion induced self-assembly process. *ACS Nano* **2012**, *6*, 2693–2703.
- (17) Worsley, M. A.; Pauzauskie, P. J.; Olson, T. Y.; Biener, J.; Satcher, J. H.; Baumann, T. F. Synthesis of graphene aerogel with high electrical conductivity. *J. Am. Chem. Soc.* **2010**, *132*, 14067–14069.
- (18) Worsley, M. A.; Olson, T. Y.; Lee, J. R. I.; Willey, T. M.; Nielsen, M. H.; Roberts, S. K.; Pauzauskie, P. J.; Biener, J.; Satcher, J. H.; Baumann, T. F. High surface area, sp²-cross-linked three-dimensional graphene monoliths. *J. Phys. Chem. Lett.* **2011**, *2*, 921–925.
- (19) Markovic, Z. M.; Babic, B. M.; Dramicanin, M. D.; Antunovic, I. D. H.; Pavlovic, V. B.; Perusko, D. B.; Markovic, B. M. T. Preparation of highly conductive carbon cryogel based on pristine graphene. *Synth. Met.* **2012**, *162*, 743–747.
- (20) Bandi, S.; Schiraldi, D. A. Glass transition behavior of clay aerogel/poly(vinyl alcohol) composites. *Macromolecules* **2006**, *39*, 6537–6545.
- (21) Ge, D. T.; Yang, L. L.; Li, Y.; Zhao, J. P. Hydrophobic and thermal insulation properties of silica aerogel/epoxy composite. *J. Non-Cryst. Solids* **2009**, *355*, 2610–2615.
- (22) Gupta, N.; Ricci, W. Processing and compressive properties of aerogel/epoxy composites. *J. Mater. Process. Technol.* **2008**, *198*, 178–182.
- (23) Zhang, B.; Dong, X. M.; Song, W.; Wu, D. C.; Fu, R. W.; Zhao, B.; Zhang, M. Q. Electrical response and adsorption performance of novel composites from polystyrene filled with carbon aerogel in organic vapors. *Sens. Actuators, B: Chem.* **2008**, *132*, 60–66.
- (24) Du, A.; Zhou, B.; Li, Y.; Li, X.; Ye, J.; Li, L.; Zhang, Z.; Gao, G.; Shen, J. Aerogel: A potential three-dimensional nanoporous filler for resins. *J. Reinf. Plast. Compos.* **2011**, *30*, 912–921.
- (25) Ji, X.; Lee, K. T.; Nazar, L. F. A highly ordered nanostructured carbon-sulphur cathode for lithium-sulphur batteries. *Nat. Mater.* **2009**, *8*, 500–506.
- (26) Kim, K. H.; Vural, M.; Islam, M. F. Single-Walled Carbon Nanotube Aerogel-Based Elastic Conductors. *Adv. Mater.* **2011**, DOI: 10.1002/adma.201100310.
- (27) Gui, X.; Li, H.; Zhang, L.; Jia, Y.; Liu, L.; Li, Z.; Wei, J.; Wang, K.; Zhu, H.; Tang, Z.; Wu, D.; Cao, A. A facile route to isotropic conductive nanocomposites by direct polymer infiltration of carbon nanotube sponges. *ACS Nano* **2011**, *5*, 4276–4283.
- (28) Sun, H.; Xu, Z.; Gao, C. Multifunctional, ultra-flyweight, synergistically assembled carbon aerogels. *Adv. Mater.* **2013**, *25*, 2554–2560.
- (29) Bryning, M. B.; Milkie, D. E.; Islam, M. F.; Hough, L. A.; Kikkawa, J. M.; Yodh, A. G. Carbon nanotube aerogels. *Adv. Mater.* **2007**, *19*, 661–664.
- (30) Boday, D. J.; Muriithi, B.; Stover, R. J.; Loy, D. A. Polyaniline nanofiber-silica composite aerogels. *J. Non-Cryst. Solids* **2012**, *358*, 1575–1580.
- (31) Parviz, D.; Das, S.; Ahmed, H. S. T.; Irin, F.; Bhattacharia, S.; Green, M. J. Dispersions of non-covalently functionalized graphene with minimal stabilizer. *ACS Nano* **2012**, *6*, 8857–8867.
- (32) Wu, C.; Huang, X.; Wang, G.; Lv, L.; Chen, G.; Li, G.; Jiang, P. Highly conductive nanocomposites with three-dimensional, compactly interconnected graphene networks via a self-assembly process. *Adv. Funct. Mater.* **2013**, *23*, 506–513.
- (33) Zaman, I.; Kuan, H.-C.; Meng, Q.; Michelmoro, A.; Kawashima, N.; Pitt, T.; Zhang, L.; Gouda, S.; Luong, L.; Ma, J. A Facile Approach

to Chemically Modified Graphene and its Polymer Nanocomposites. *Adv. Funct. Mater.* **2012**, 22, 2735–2743.

(34) Wu, L.; Lv, X.; Zhang, C. Effect of modified graphene addition on the electrical properties of epoxy resin composite. *Adv. Mater. Res.* **2011**, 239–242, 55–58.

(35) Saw, W. P. S.; Mariatti, M. Properties of synthetic diamond and graphene nanoplatelet-filled epoxy thin film composites for electronic applications. *J. Mater. Sci.: Mater. Electron.* **2012**, 23, 817–824.

(36) Liang, J.; Wang, Y.; Huang, Y.; Ma, Y.; Liu, Z.; Cai, F.; Zhang, C.; Gao, H.; Chen, Y. Electromagnetic interference shielding of graphene/epoxy composites. *Carbon* **2009**, 47, 922–925.

(37) Mukai, S. R.; Nishihara, H.; Yoshida, T.; Taniguchi, K.; Tamon, H. Morphology of resorcinol-formaldehyde gels obtained through ice-templating. *Carbon* **2005**, 43, 1563–1565.

(38) Mukai, S. R. Controlling the morphology of carbon gels. *Microporous Mesoporous Mater.* **2003**, 63, 43–51.

(39) Zou, J. H.; Liu, J. H.; Karakoti, A. S.; Kumar, A.; Joung, D.; Li, Q. A.; Khondaker, S. I.; Seal, S.; Zhai, L. Ultralight multiwalled carbon nanotube aerogel. *ACS Nano* **2010**, 4, 7293–7302.

(40) Das, S.; Irin, F.; Ma, L.; Bhattacharia, S. K.; Hedden, R. C.; Green, M. J. Rheology and morphology of pristine graphene/polyacrylamide gels. *ACS Appl. Mater. Interfaces* **2013**, DOI: 10.1021/am402185r.

(41) Husing, N.; Schubert, U. Aerogels airy materials: Chemistry, structure, and properties. *Angew. Chem., Int. Ed.* **1998**, 37, 23–45.

(42) Zhou, C.; Wu, Q. A novel polyacrylamide nanocomposite hydrogel reinforced with natural chitosan nanofibers. *Colloids Surf., B: Biointerfaces* **2011**, 84, 155–162.

(43) Zhou, C.; Wu, Q.; Yue, Y.; Zhang, Q. Application of rod-shaped cellulose nanocrystals in polyacrylamide hydrogels. *J. Colloid Interface Sci.* **2011**, 353, 116–123.